ELECTRONIC SUPPLEMENTARY MATERIAL 1

NEW INSIGHT INTO THE RELATIONSHIPS BETWEEN STRUCTURAL AND FTIR SPECTROSCOPIC FEATURES OF KAOLINITES. Clays and Clay Minerals.

Victor A. Drits[1], Bella B. Zviagina[1]*, Boris A. Sakharov[1], Olga V. Dorzhieva[2], and Aleksandr T. Savichev[1].

[1] Geological Institute of the Russian Academy of Science, Pyzhevsky per. 7, 119017 Moscow, Russia

[2] Institute of Ore Deposits, Petrography, Mineralogy, and Geochemistry of the Russian Academy of Science, Staromonetny per. 35, 7, 119017 Moscow, Russia

ORCID:

V.A. Drits: 0000-0001-8253-5153
B.B. Zviagina: 0000-0001-6493-4361
B.A. Sakharov: 0000-0002-1908-6778
A.T. Savichev: 0000-0002-6434-7148

* Corresponding author: Geological Institute of the Russian Academy of Science, Pyzhevsky per. 7, 119017 Moscow, Russia, e-mail: zbella2001@yahoo.com

Table of Contents

Section I. Procedure for the determination of the unit-cell parameters and atomic coordinates of the kaolinite orthogonal unit cell.

The mutual arrangement of the right- and left-hand oblique cells and layer displacement vectors $\boldsymbol{t_1}$ and $\boldsymbol{t_2}$, which correspond to the individual kaolinite enantiomorphs related by a mirror plane, as well as the layer orthogonal cell with the a_0 axis coinciding with the mirror plane, are shown in Fig. 1. The parameters of the oblique cell (a, b, γ) refined by Bish and von Dreele (1989) are related to the parameters a_0 and b_0 of the orthogonal unit cell by the equations (Bookin et al., 1989, Drits *et al.*, 2018)

$$4a^2 = a^2 + b^2 - 2ab\cos\gamma$$

$$4a_0^2 = a^2 + b^2 - 2ab\cos(180 - \gamma) \qquad \text{(S1)}$$

$$4a^2 = a_0^2 + b_0^2;\ 4b^2 = b_0^2 + 9a_0^2$$

$$2a_0^2 = b^2 - a^2$$

According to Drits *et al.* (2018), to provide accurate correlation between the parameters of the refined oblique and orthogonal layer cells, the value of the a parameter is reduced by one estimated standard deviation (1σ), and the b and γ values are increased by 1σ and 1.5σ, respectively. From equations (1), the corrected oblique layer cell parameters (a = 5.1553 Å, b = 8.950 Å, γ = 89.825º) correspond to the orthogonal layer cell with a_0 = 5.1689 Å, b_0 = 8.9214 Å, γ = 90º).

The Cartesian atomic coordinates of the orthogonal (x_0, y_0) and the oblique (x, y) unit cells are related by

$$x_0 = 0.5x + 1.5y;\ y_0 = -0.5x + 0.5y;\ z_0 = z \qquad \text{(S2)}$$

These equations were used to calculate the atomic coordinates (x_0, y_0, z_0) of the orthogonal unit cell having *Cm* symmetry (Table S1) (see Drits *et al.*, 2018 for details). Similarly, the components of the layer displacement along the [100] and [010] directions, -0.3683a and -0239b, of the oblique layer cell were transformed, using equation 2, into the corresponding components, -0.2200a_0 and 0.1722b_0, of the layer displacement of the orthogonal

cell. The layer displacement vector $\boldsymbol{t}_{01} = -0.2200a_0 + 0.1722b_0$ corresponds to the left-hand defect-free kaolinite structure. To obtain the right-hand defect-free structure, the layer displacement vector $\boldsymbol{t}_{02} = -0.2200a_0 - 0.1722b_0$, which is related to $\boldsymbol{t}_{01}$ by a mirror plane, should be used (Fig. S1).

Table S1. Atomic coordinates of the orthogonal layer unit cell having *Cm* symmetry.

Atom	x_0	y_0	z_0
Al_1	0.7881	0.1655	0.4710
Al_2	0.7881	- 0.1655	0.4710
Si_1	0.4844	0.1713	0.0911
Si_2	0.4844	- 0.1713	0.0911
O_1	0.4838	0.1911	0.3172
O_2	0.4838	- 0.1911	0.3172
O_3	0.7492	0.2336	0.0016
O_4	0.4445	0.0001	0.0024
O_5	0.7492	- 0.2336	0.0016
$(OH)_1$	0.4093	0.5	0.3220
$(OH)_2$	0.5990	- 0.3104	0.6065
$(OH)_3$	0.5990	0.3104	0.6065
$(OH)_4$	0.1683	0.5	0.6094

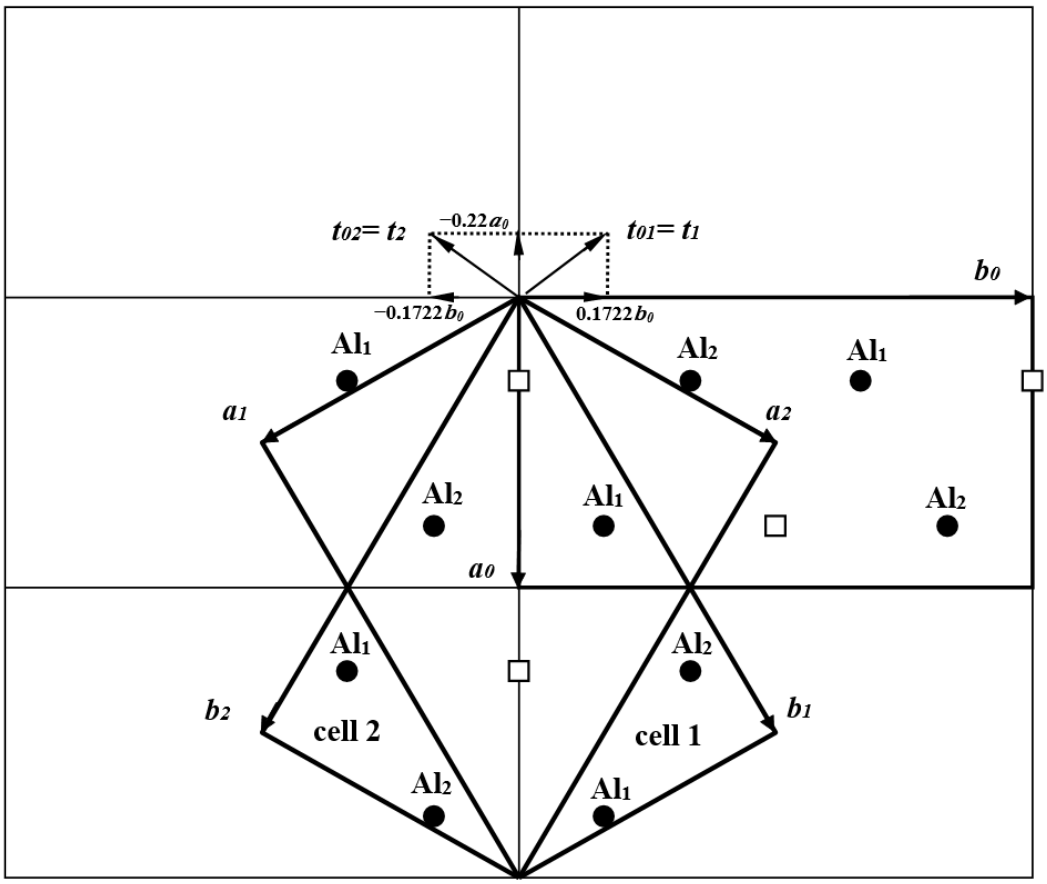

Fig. S1. Mutual arrangement of two oblique layer unit cells (cell 1 and cell 2) and the orthogonal unit cell describing the two-dimensional periodicity of the kaolinite layer. Cells 1 and 2 are related by a mirror plane passing through the a_0 axis and normal to the b_0 axis of the orthogonal layer unit cell. The layer displacement vectors $\boldsymbol{t_1}$ and $\boldsymbol{t_2}$ form the right- and left-handed kaolinite enantiomorphs, respectively; $\boldsymbol{t}_{01} = -0.2200a_0 + 0.1722b_0$ and $\boldsymbol{t}_{02} = -0.2200a_0 - 0.1722b_0$.

Section II. Modelling of the XRD patterns.

To simulate diffraction features for the studied kaolinite samples, the atomic coordinates obtained for the kaolinite layers having the orthogonal unit cell, *C*m layer symmetry, and $\boldsymbol{t}_{01}$ and $\boldsymbol{t}_{02}$ layer displacements were used in the computer program of Sakharov and Naumov (1982, 1983), which is based on the algorithms described by Drits and Tchoubar (1990). An advantage of the program is that the intensity distribution is calculated for the whole XRD pattern range using the same set of structure parameters. In addition, model structures may contain an arbitrary number of various types of stacking faults, and their distributions may correspond to an arbitrary value of the short-range order factor *R* (Drits and Tchoubar, 1990).

The XRD patterns were calculated for a model of a physical mixture of two populations of crystallites having contrasting structural order, i.e. very low and very high contents of stacking faults resulting from interstratified layer displacements, and described by the above the set of structural parameters. In these models, crystallites or coherent scattering domains (CSDs) consisting of layers parallel to the *ab* plane had a disk-like shape and various radii that occurred with equal probability. The CSD thicknesses were distributed log-normally along the *c** axis using the regression given by Drits *et al.* (1997). The mean and maximum thicknesses of CSDs having log-normal distribution were used as variable parameters. Corrections for instrumental factors, such as horizontal and vertical beam divergence, length, width and sample thickness, were made according to the recommendations of Drits *et al*. (1993) and Reynolds (1986). If the layer displacement is not fixed in length, the variation of the length around the average value is described by Gaussian distribution expressed by the term

$$exp\left[-\pi^2\left(h^2\delta_x^2 + k^2\delta_y^2 + l^2\delta_z^2\right)\right], \quad \text{(S3)}$$

where δ_x, δ_y and δ_z are the characteristic widths (in fractions of the unit cell parameters) of the distribution in the *a*, *b* and *c* directions, respectively.

The powder XRD patterns from kaolinite samples may differ because of the variations in the relative orientation of kaolinite particles. The degree of particle preferred orientation was estimated by the angular parameter, α, equal to the full width at half-maximum (*FWHM*) of the particle distribution (Drits and Tchoubar, 1990). For each model, two XRD patterns were calculated using Cu-Kα_1 and Cu-Kα_2 wavelengths and summed in the ratio 2:1, respectively. When the structural parameters for each model are fixed, the program automatically seeks the best agreement (minimum R_p factor) between the experimental and calculated XRD patterns by varying the contents of each population in the model.

Layer displacements for XRD modeling. Application of the trial-and-error approach showed that the best agreement between the experimental and calculated XRD patterns is achieved when the unit-cell parameters and layer displacements coincide with those described

above for the *C*m layer symmetry. Because of the nearly trigonal symmetry of the kaolinite layer, a third layer displacement vector $\boldsymbol{t_0} = 0.3698a_0$ directed along the mirror plane may also exist in the kaolinite structure. The $\boldsymbol{t_{01}}$, $\boldsymbol{t_{02}}$ and $\boldsymbol{t_0}$ vectors are of equal lengths, and the CSD thickness was determined by the modeling of the whole experimental XRD pattern including basal reflection profiles. A model of a defective kaolinite structure consisting of layers of the same type is thus defined by the probabilities of the $\boldsymbol{t_{01}}$, $\boldsymbol{t_{02}}$ and $\boldsymbol{t_0}$ translations, $W_{t_{01}}$, $W_{t_{02}}$ and W_{t_0}, respectively.

REFERENCES

Drits, V.A. & Tchoubar, C. (1990). *X-ray Diffraction by Disordered Lamellar Structures* (371 pp.). Berlin, Heidelberg: Springer.

Drits, V.A., Kameneva, M.Y., Sakharov, B.A., Daynyak, L.G., Tsipurski, S.I., Smolyar, B.B., Bookin, A.S., & Salyn, A.L. (1993). *The Actual Structure of Glauconites and Related Mica-like Minerals* (189pp.) (in Russian). Novosibirsk: Nauka.

Drits, V.A., Środoń, J., & Eberl, D.D. (1997). XRD measurements of mean crystallite thickness of illite and illite/smectite: reappraisal of the Kubler index and the Scherrer equation. *Clays and Clay Minerals, 45*, 461–475.

Reynolds, R.C. Jr (1986). The Lorentz-polarization factor and preferred orientation in oriented clay aggregates. *Clays and Clay Minerals, 34*, 359–367.

Sakharov, B.A., Naumov, A.S., Drits, V.A. (1982). X-ray intensities scattered by layer structures with short-range ordering parameters S ≥ 1 and G ≥ 1. *Dokl. Akad. Nauk*, 265, 871–874 (in Russian).

Sakharov, B.A., Naumov, A.S., Drits, V.A. (1983). X-ray scattering by defect layer structures. *Kristallografia*, 28, 951–958 (in Russian).

Table S2 Structural parameters of the HOK and LOK fractions of the studied samples

***a*(Å)**	***b*(Å)**	***c**(Å)*	***γ*°**	***t*$_{01}$**	***t*$_{02}$**	***t*$_0$**
5.169	8.921	7.154	90	-0.2200*a* 0.1722*b*	-0.2200*a* -0.1722*b*	0.3698*a*

Sample	**Phase**	**C(%)**	**W$_{t01}$**	**W$_{t02}$**	**W$_{t0}$**	**W$_a$**	***δ*(*t*)**	**N**	**D(Å)**	**α°**	**qz**	**an**	***Rp***
Keok-1†	HOK	86	1	0	0	0	-	80	100 - 1100	90	+	+	18.8
	LOK	14	0.55	0.45	0	0	-	60	100 - 1100	80			
Keok-2	HOK	80	1	0	0	0	0.05*c**	70	100 - 1000	170			14.6
	LOK	20	0.55	0.45	0	0	0.05*c**	70	100 - 1000	170			
Ch-76	HOK	73	1	0	0	0	0.05*c**	35	100 - 900	110			12.7
	LOK	27	0.55	0.45	0	0	0.05*c**	35	100 - 900	110			
Keok-3	HOK	69	0.98	0.02	0	0	-	65	100 - 1100	90			11.4
	LOK	31	0.55	0.45	0	0	0.02*a*	65	100 - 1100	90			
E-4	HOK	68	0.98	0.02	0	0	-	65	100 - 1000	140			8.3
	LOK	32	0.55	0.45	0	0	-	65	100 - 1000	140			
Keok-4	HOK	68	1	0	0	0	0.05*c**	60	100 - 800	120	+		11.4
	LOK	32	0.55	0.45	0	0	0.05*c**	60	100 - 800	120			
An	HOK	59	0.98	0.02	0	0	0.02*a* 0.05*c**	28	100 - 900	70	+		21.3
	LOK	41	0.55	0.43	0.02	0.05	0.02*a* 0.05*c**	28	100 - 900	70			
Dec	HOK	55	0.98	0.02	0	0	-	50	100 - 900	120	+		9.8
	LOK	45	0.55	0.45	0	0	-	50	100 - 900	120			
Pr	HOK	55	0.98	0.02	0	0	0.02*a* 0.05*c**	18	100 - 900	60			11.7
	LOK	45	0.55	0.43	0.02	0.05	0.02*a* 0.05*c**	18	100 - 900	60			
Ch-67	HOK	54	0.98	0.02	0	0	0.025*a*	30	100 - 900	100	+		9.3
	LOK	46	0.55	0.45	0	0.04	-	30	100 - 900	100			
Sd	HOK	41	0.98	0.02	0	0.065	0.025*a* 0.05*c**	18	100 – 900	75	+		10.3
	LOK	59	0.60	0.38	0.02	0.05	0.025*a* 0.05*c**	18	100 – 900	75			
Vl	HOK	37	0.98	0.02	0	0	0.02*a*	18	100 - 700	90			9.7
	LOK	63	0.55	0.43	0.02	0.05	0.02*a*	18	100 - 700	90			
KGa-1b	HOK	37	0.98	0.02	0	0	0.025*a*	25	100 - 800	160		+	10.3
	LOK	63	0.55	0.45	0	0.04	0.025*a*	25	100 - 800	160			
Sm	HOK	36	0.97	0.03	0	0	0.02*a* 0.05*c**	18	100 – 700	180			9.3
	LOK	64	0.55	0.43	0.02	0.05	0.02*a*	18	100 – 700	180			
KGa-1	HOK	27	0.97	0.03	0	0	0.03*a* 0.05*c**	45	200 - 800	90		+	10.0
	LOK	73	0.58	0.37	0.05	0.05	0.02*a* 0.02*b*	45	200 - 800	90			
G-5	HOK	18	0.98	0.02	0	0	0.05*c**	18	100 - 700	110			11.3
	LOK	82	0.55	0.40	0.05	0.05	0.02*a* 0.05*c**	18	100 - 700	110			
Im	HOK	18	0.98	0.02	0	0	0.02*a* 0.05*c**	18	100 - 700	100	+		11.0
	LOK	82	0.55	0.43	0.02	0.05	0.02*a* 0.05*c**	18	100 - 700	100			
KGa-2	HOK	4	0.98	0.02	0	0	0.02*a*	20	100 - 700	120		+	10.9
	LOK	96	0.58	0.37	0.05	0.07	0.03*a*	20	100 - 700	120			

† the sample contains a small amount (3%) of dickite; qz and an correspond to quartz and anatase, respectively

Fig. S2. The best possible agreement between the experimental XRD patterns of kaolinite samples under study (open circles) and those obtained by the optimal summation of the modeled XRD patterns of the HOK and LOK phases (solid line): (a) samples Keok-1, Keok-2, Ch-76; (b) samples Keok-3, E-4; Keok-3; (c) samples An, Dec, Pr; (d) samples Ch-67, Sd, Vl; (e) samples KGa-1b, Sm, KGa-1; (f) samples G-5, Im, KGa-2.

Fig. S2a

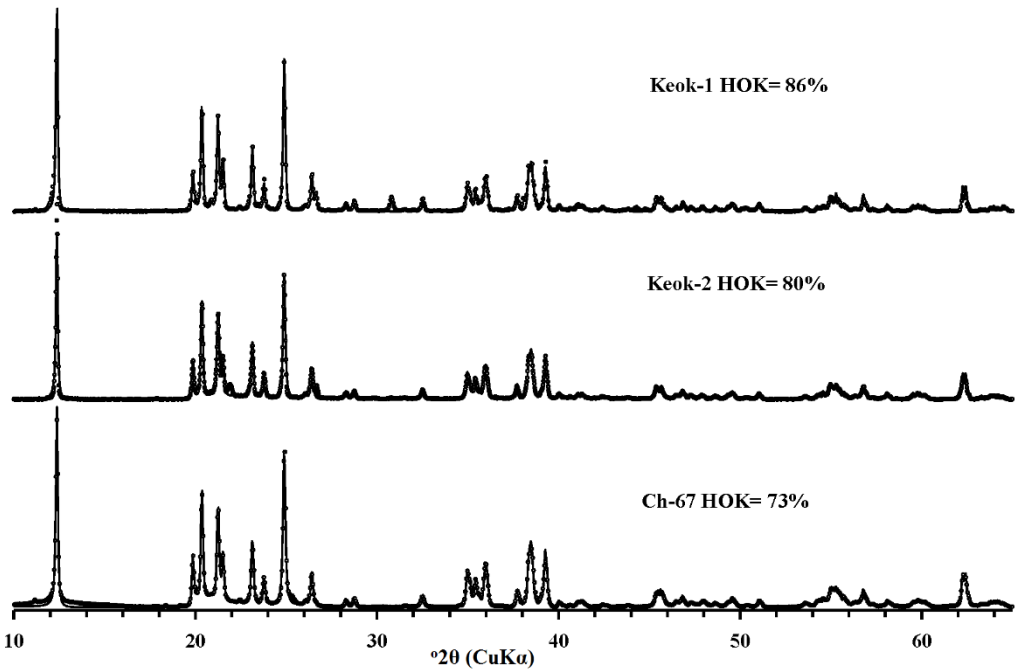

Fig. S2b

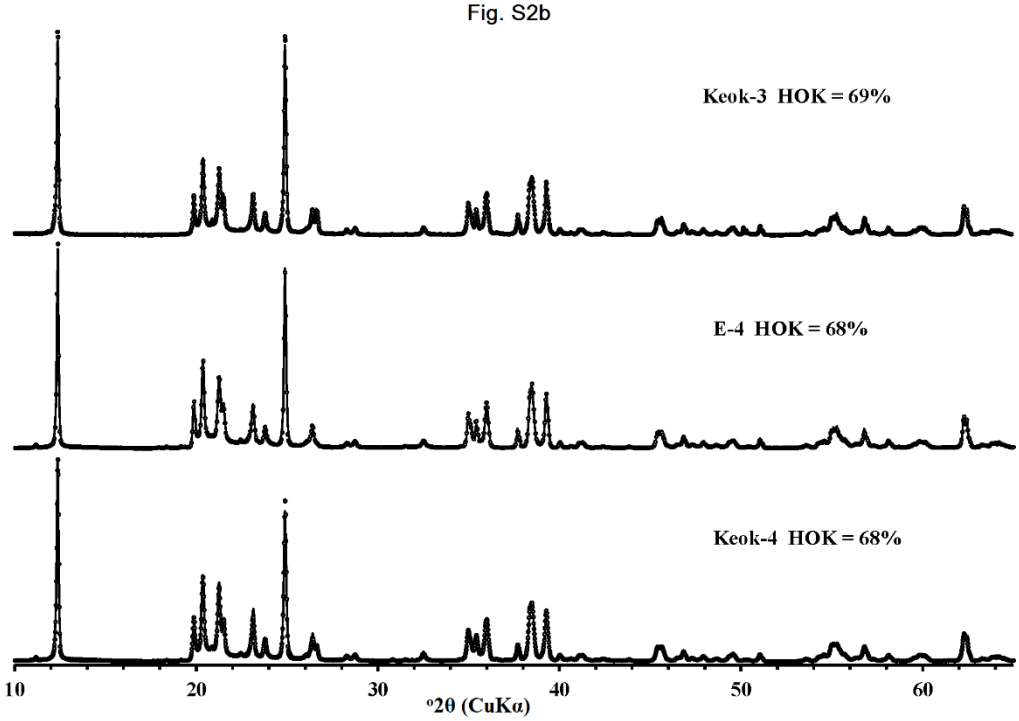

Fig. S2c

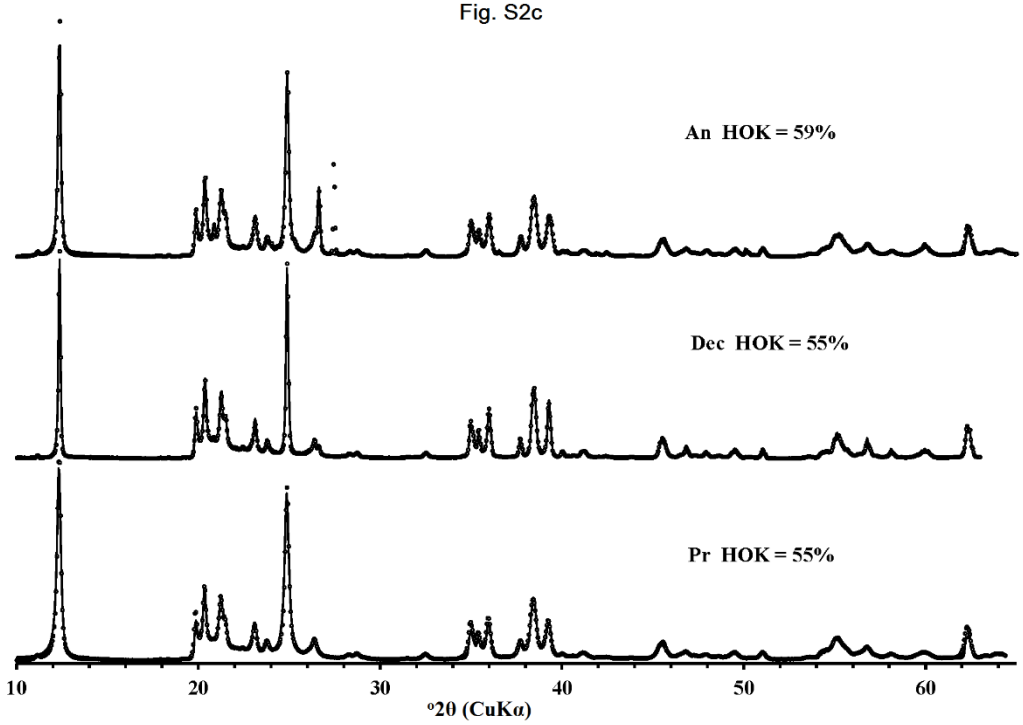

Fig. S2d

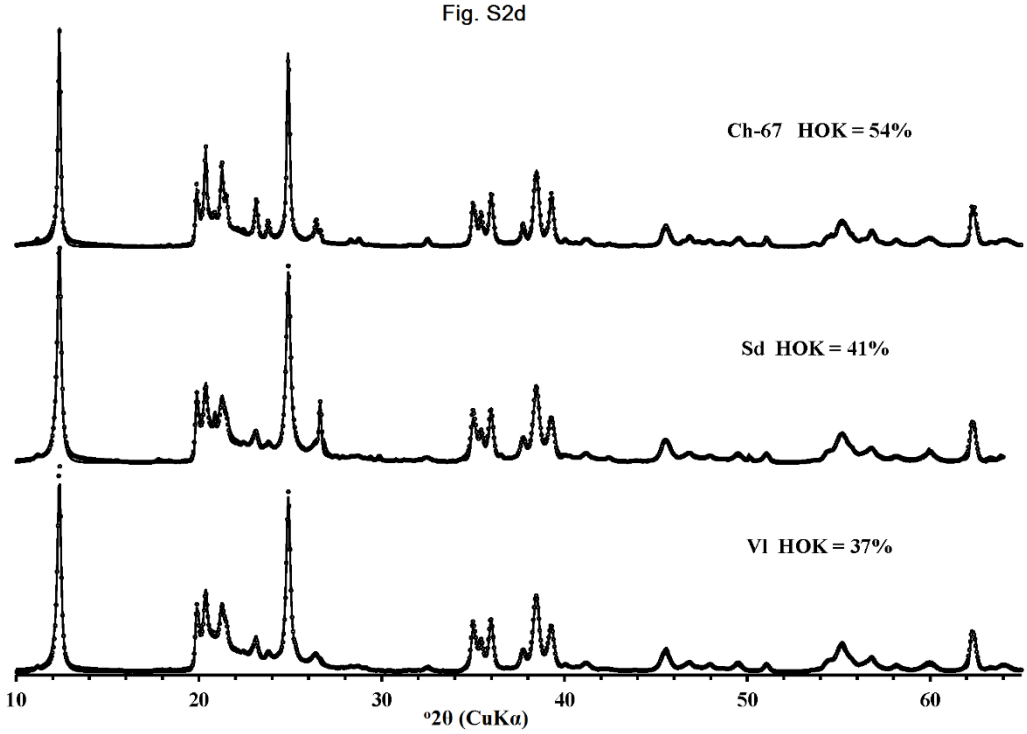

Fig. S2e

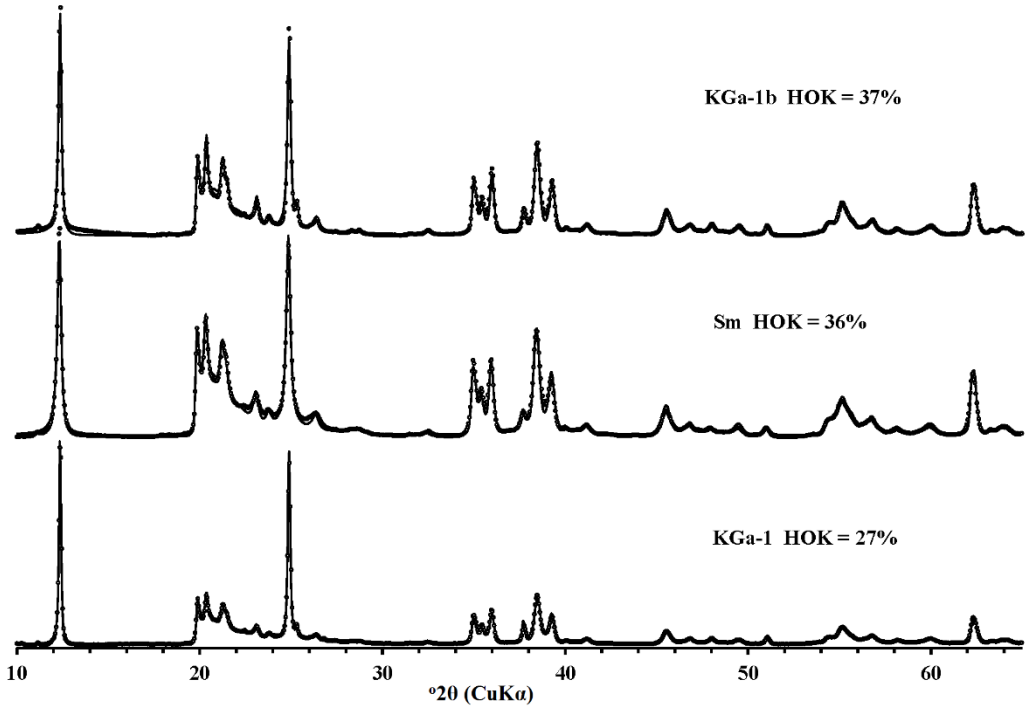

Fig. S2f

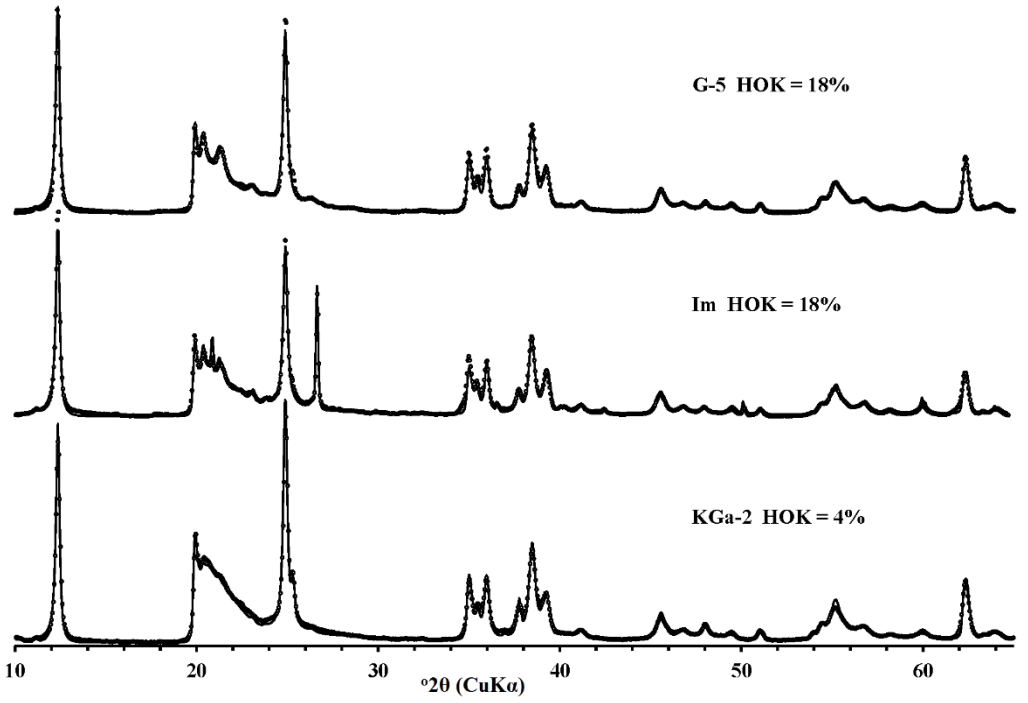

Section III. Fig. S3. Decomposition and curve-fitting of the FTIR spectra of the kaolinite samples in the OH-stretching region: (a) Keok-1, Keok-2, Ch-76, Keok-3, E-4, Keok-4; (b) An, Dec, Pr, Ch-67, Sd, Vl; (c) KGa-1b, Sm, KGa-1, G-5, Im, KGa-2, Capim. PS group corresponds to particle size group in Tables 1, 2.

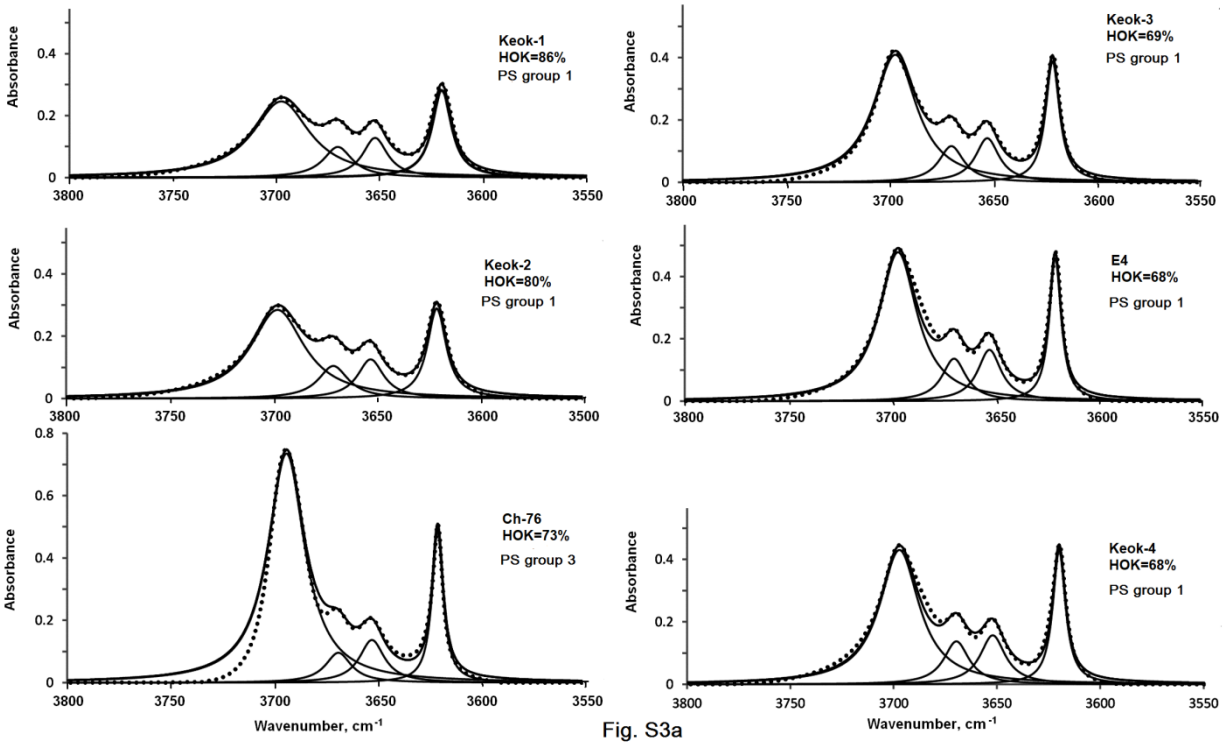

Fig. S3a

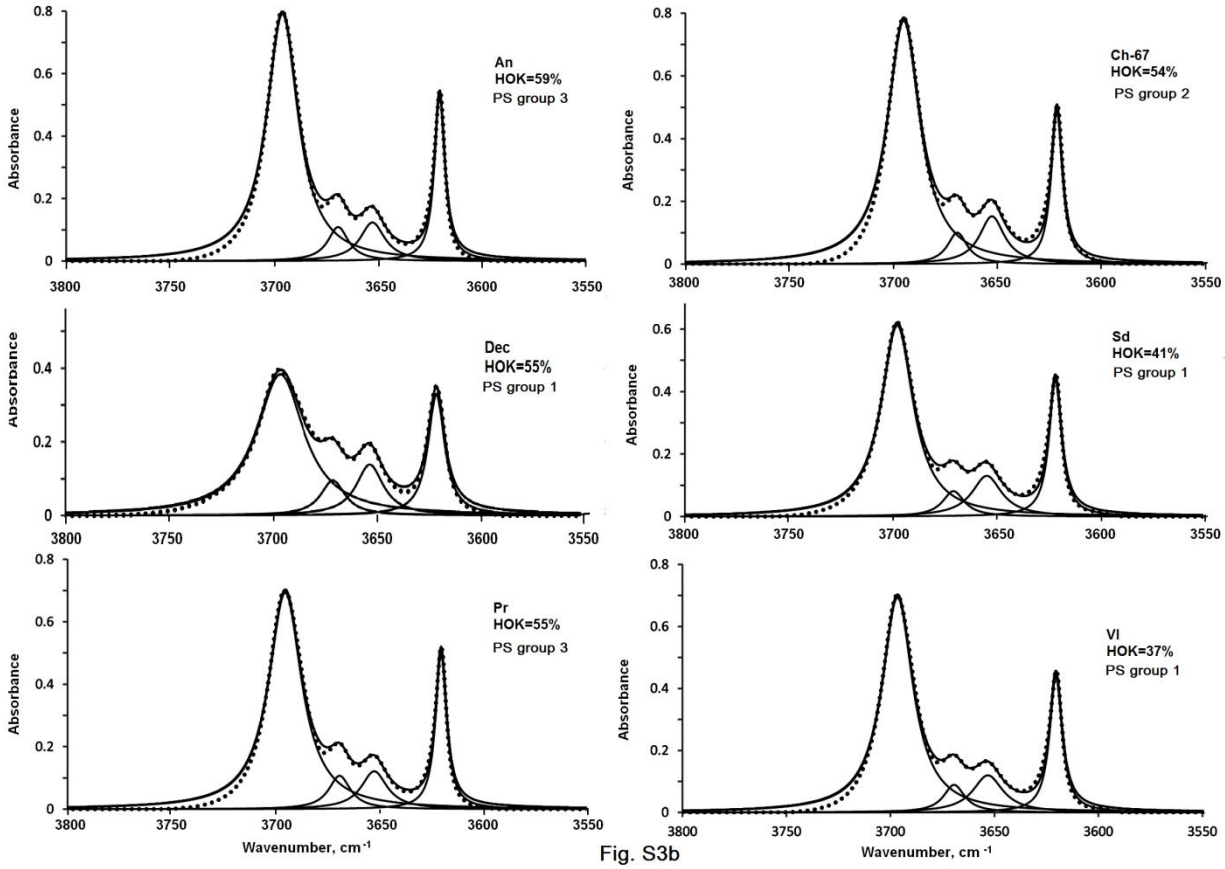
An
HOK=59%
PS group 3
Ch-67
HOK=54%
PS group 2
Dec
HOK=55%
PS group 1
Sd
HOK=41%
PS group 1
Pr
HOK=55%
PS group 3
Vl
HOK=37%
PS group 1
Absorbance
Wavenumber, cm-1

Fig. S3b

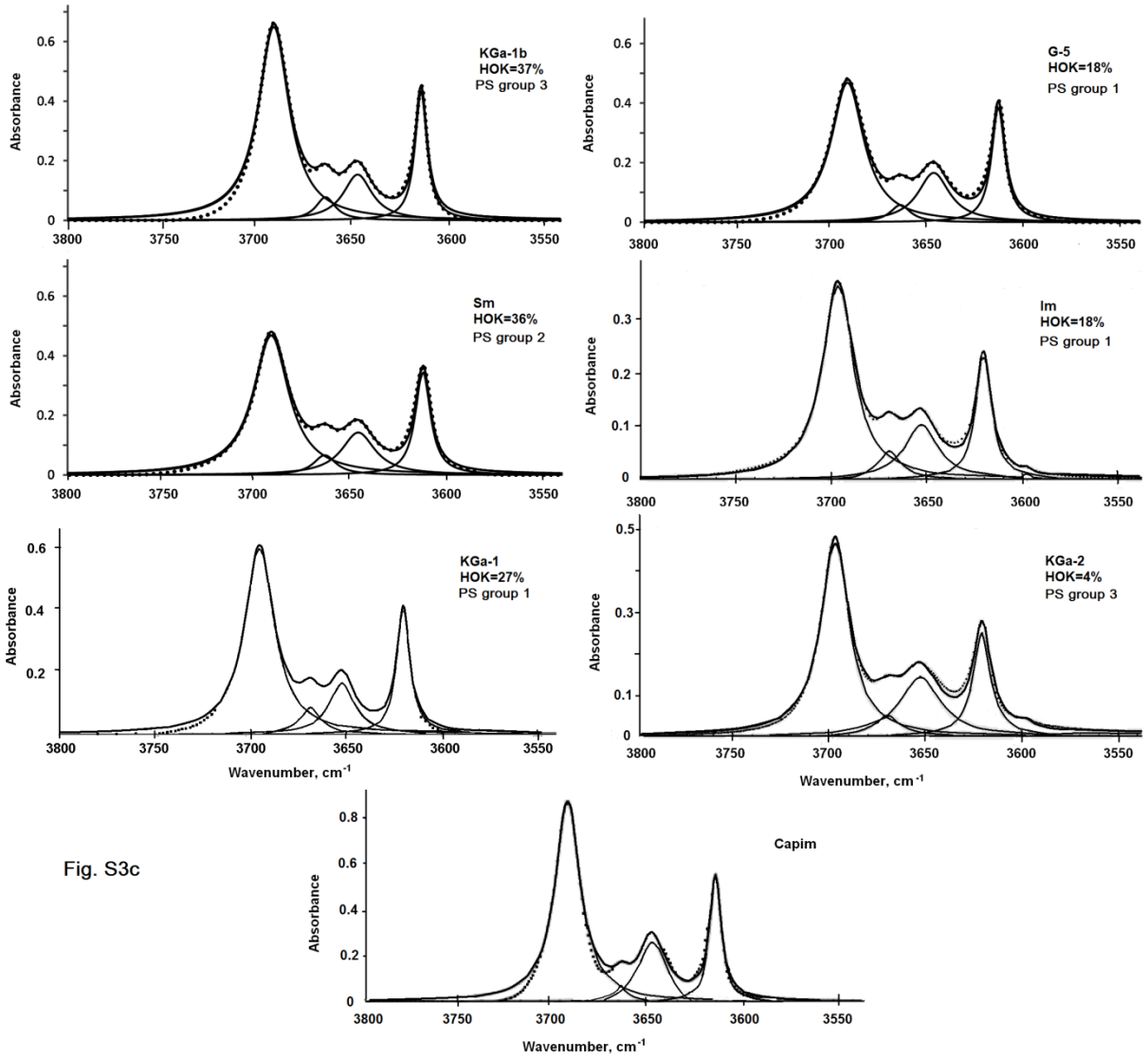

Fig. S3c

Section IV. FTIR spectroscopy: Supplementary Discussion

Relationships between the HOK phase contents and the FWHM values: the v_2 and v_3 bands.

The *FWHM* values of the v_3 bands for the samples having HOK ≥ 50% are segregated within a narrow range from ~14 to 16 cm^{-1}, whereas for the other samples, the *FWHM*(v_3) values tend to increase with decreasing HOK content within a much wider range from ~17 to ~24 cm^{-1} (Fig. S4a). In contrast, the *FWHM*(v_2) values for the samples with HOK ≥ 50% decrease consistently with decreasing HOK content within rather a wide range (17.6-11.7 cm^{-1}) (Fig. S4b). This trend is realized in the transition from samples composed by coarse crystallites (Keok-2) to those consisting of fine crystallites (Ch-67). The *FWHM*(v_2) values of the samples

with HOK < 50% are scattered within rather a narrow range from 11.3 to 13.8 cm^{-1} in comparison with broader bands for the samples composed of coarse crystallites and having HOK ≥ 50%. (Fig. 4b).

The mutual distribution of the *FWHM*(v_2) and *FWHM*(v_3) values (Fig. S4c) shows that the decrease in the HOK contents in the samples with HOK ≥ 50% should be accompanied by an increase in the *FWHM*(v_3)/*FWHM*(v_2) ratios because of the narrow variation range of the *FWHM*(v_3) values in combination with a consistent decrease in the *FWHM*(v_2) values. The samples with lower HOK contents should show the same trend because of the combination of rather a narrow variation range for FWHM(v_2) with the broadening of the v_3 bands observed in the series of samples from Sd to KGa-2 (Fig. S4c). In the light of these observations, the application of the same approach, as used for the description of the relationships between the HOK contents and the *FWHM*(ν_1)/*FWHM*(ν_4) values, implies that the *FWHM*(ν_3)/*FWHM*(ν_2) ratios and HOK contents should be related by a linear dependence. Indeed, the relationship between the *FWHM*(v_3)/*FWHM*(v_2) and the HOK values is described by the regression:

$$HOK = -72.917[FWHM(v_3)/FWHM(v_2)] + 142.360 \qquad (S4)$$

(R^2 = 0.974, Fig. S4d). Despite the wide range of the *FWHM* (v_3) and *FWHM* (v_2) distribution, the HOK phase contents control, therefore, the relationship between the particular values of *FWHM* (v_2) and *FWHM* (v_3) corresponding to each particular content of the HOK phase.

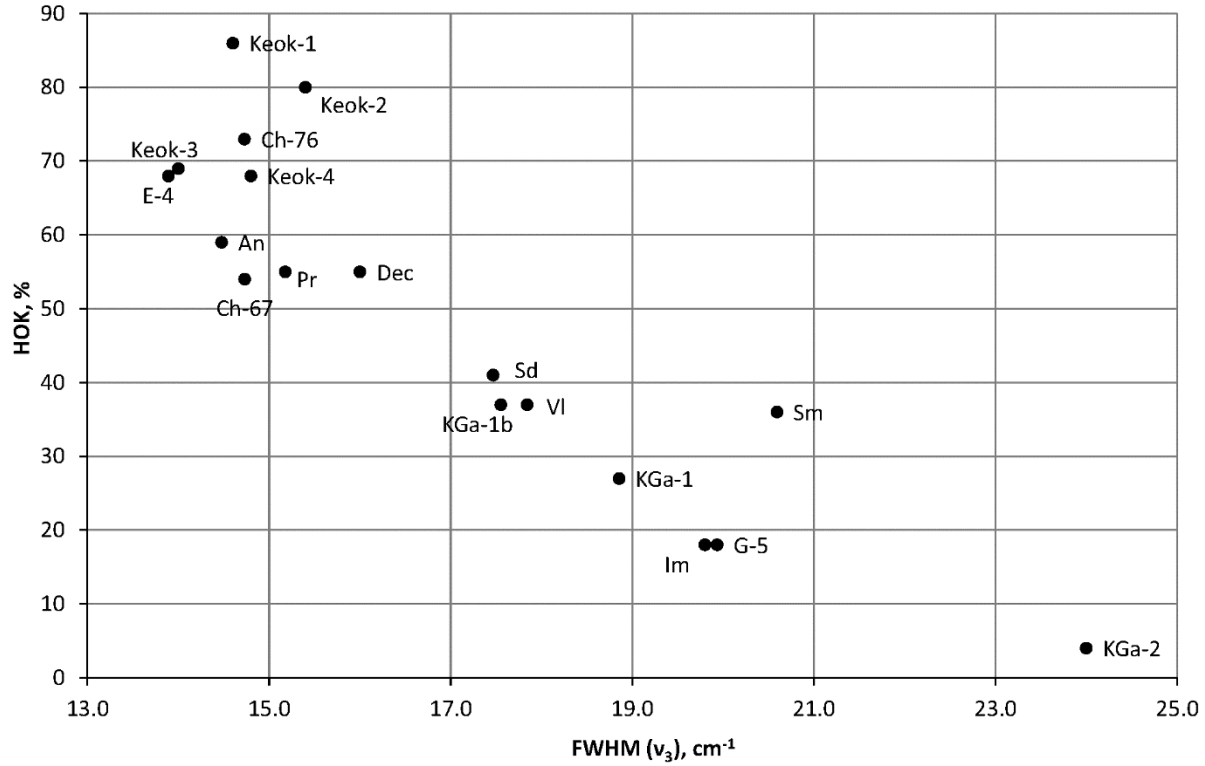

Fig. S4a. The HOK contents plotted *vs*. *FWHM*(ν_3)

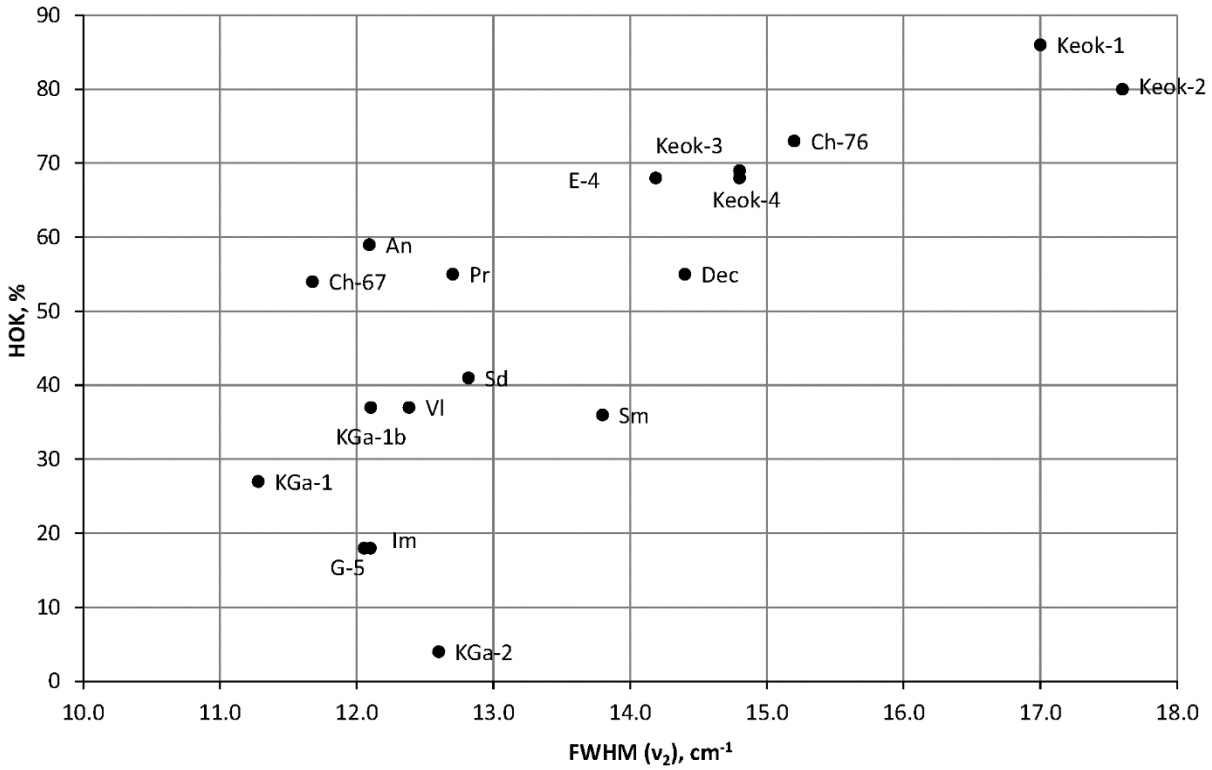

Fig. S4b. The HOK contents plotted *vs*. *vs FWHM*(ν_2)

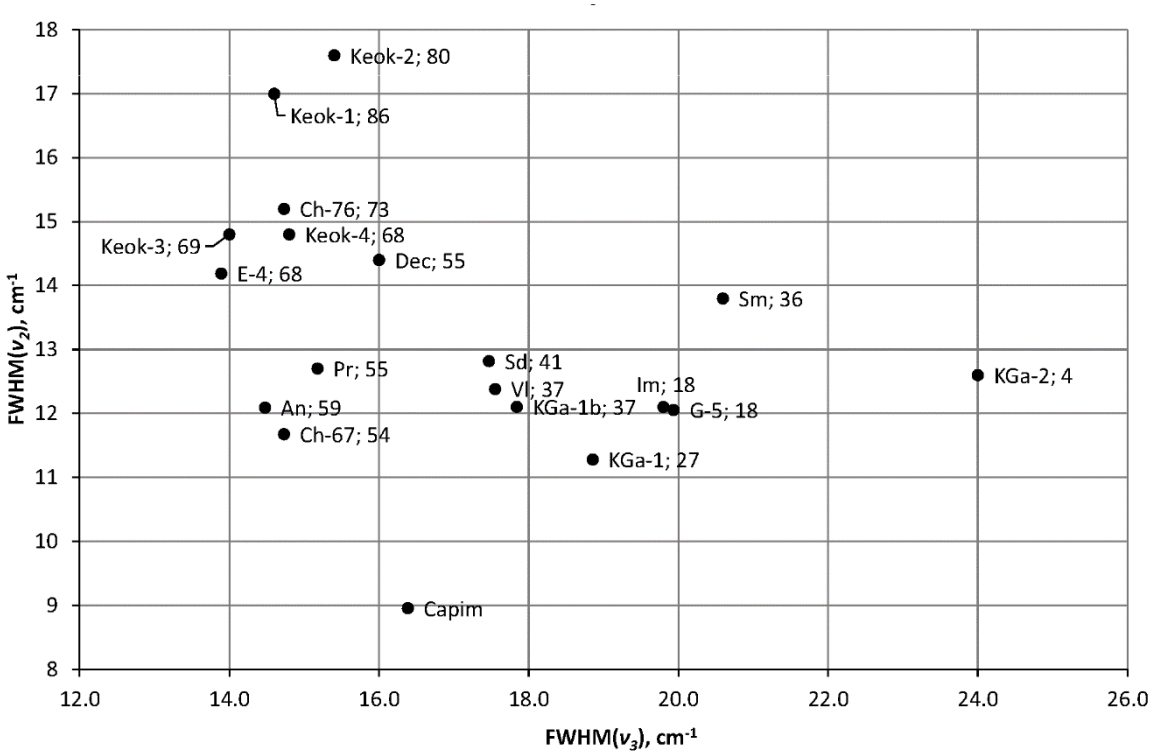

Fig. S4c. The *FWHM*(ν_2) values plotted *vs*. *FWHM*(ν_3).

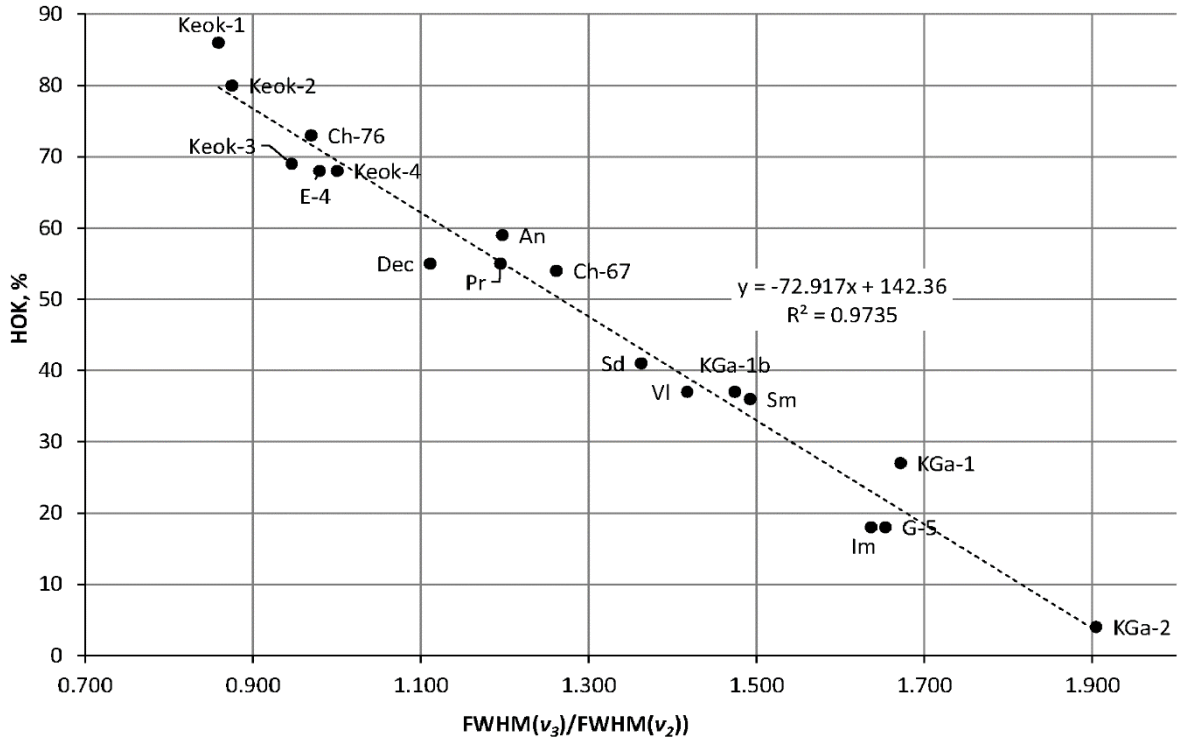

Fig. S4d. The HOK contents plotted *vs*. the *FWHM*(ν_3)/*FWHM*(ν_2) ratios.